SCIENCE CHINA
Technological Sciences

Deformation mode-determined misorientation and microstructural characteristics in rolled pure Zr sheet

LinJiang CHAI, JiYing XIA, Yan ZHI, YinNing GOU, LiangYu CHEN, ZhiNan YANG and Ning GUO

Citation: SCIENCE CHINA Technological Sciences **61**, 1346 (2018); doi: 10.1007/s11431-018-9292-1

View online: http://engine.scichina.com/doi/10.1007/s11431-018-9292-1

View Table of Contents: http://engine.scichina.com/publisher/scp/journal/SCTS/61/9

Published by the Science China Press

SCIENCE CHINA
Technological Sciences

SCIENCE CHINA
Technological Sciences

•Article•

September 2018 Vol.61 No.9: 1346–1352
https://doi.org/10.1007/s11431-018-9292-1

Deformation mode-determined misorientation and microstructural characteristics in rolled pure Zr sheet

CHAI LinJiang[1*], XIA JiYing[1], ZHI Yan[1], GOU YinNing[1], CHEN LiangYu[2], YANG ZhiNan[3*] & GUO Ning[4*]

[1] *College of Materials Science and Engineering, Chongqing University of Technology, Chongqing 400054, China;*
[2] *School of Science, Jiangsu University of Science and Technology, Zhenjiang 212003, China;*
[3] *National Engineering Research Center for Equipment and Technology of Cold Strip Rolling, Yanshan University, Qinhuangdao 066004, China;*
[4] *Faculty of Materials and Energy, Southwest University, Chongqing 400715, China*

Received February 22, 2018; accepted May 28, 2018; published online August 2, 2018

In this work, commercially pure Zr sheets were subjected to β air cooling and then rolled to different reductions (10% and 50%) at room temperature. Microstructures of both the β-air-cooled and the rolled specimens were well characterized by electron channelling contrast imaging and electron backscatter diffraction techniques, with special attentions paid to their misorientation characteristics. Results show that the β-air-cooled specimen owns a Widmanstätten structure featured by lamellar grains with typical phase transformation misorientations. The 10% rolling allows prismatic slip and tensile twinning ({11-21}<11-2-6> and {10-12}<10-11>) to be activated profusely, which produce new low-angle (~3°–5°) and high-angle (~35° and ~85°) misorientation peaks, respectively. After increasing the rolling reduction to 50%, twinning is suppressed and dislocation slip becomes the dominant deformation mode, with the lamellar grains highly elongated and aligned towards the rolling direction. Meanwhile, only one strong low-angle misorientation peak related to the prismatic slip is presented in the 50%-rolled specimen, with all other peaks disappeared. Analyses on local misorientations reveal that hardly any residual strains exist in the β-air-cooled specimen, which should be related to their sufficient relaxation during slow cooling. Residual strains introduced by 10% rolling are heterogeneously distributed near grain/twin boundaries while heavier deformation (50% rolling) produces much larger residual strains pervasively existing throughout the specimen microstructure.

pure Zr, rolling, misorientation, twinning, electron backscatter diffraction

Citation: Chai L J, Xia J Y, Zhi Y, et al. Deformation mode-determined misorientation and microstructural characteristics in rolled pure Zr sheet. Sci China Tech Sci, 2018, 61: 1346–1352, https://doi.org/10.1007/s11431-018-9292-1

1 Introduction

Zr-based alloys have wide applications in nuclear, biomedical, and chemical industries because of attractive properties like low neutron absorption, excellent biocompatibility and good corrosion resistance [1–3]. During typical fabrications of most Zr alloy materials, a β cooling is often employed and followed by multiple-step hot/cold work and annealing [4–6]. To reach reliable property control, sufficient knowledge on microstructural characteristics evolved during such processings is necessarily required, with much already documented in literature by earlier researchers. Specifically, grain sizes and morphologies in many β-cooled Zr alloys with either martensite or Widmanstätten structures have been extensively studied [7–12]. Evolutions of structures, sizes and number densities of second phase particles in various newly developed Zr alloys are also the subject of plenty of

* Corresponding authors (email: chailinjiang@cqut.edu.cn; zhinanyang@ysu.edu.cn; guoning_1000@163.com)

investigations [13–18]. In recent years, characterization of deformed grain structures and their recrystallization behaviors of Zr materials have attracted a large number of attentions as well [19–24].

Misorientation has long been recognized to be another important microstructural parameter and can play a key role in influencing properties that depend on grain-boundary networks. In contrast with continuously active misorientation studies in cubic materials [25,26], misorientation characteristics in materials with a hexagonal close packed (hcp) structure have far less been explored [27,28]. The case is even worse for commercial Zr alloys which present hcp α phase in most processing stages. Interestingly, recent work revealed that unique misorientation distributions would be presented in β-cooled Zr alloys [29,30]. How will such misorientation characteristic evolve during subsequent processings along with the underlying mechanism is also of great interest to be further explored. Such investigations are believed to be capable of not only deepening our understanding on misorientation features of hcp metals but also providing some direct insights into better microstructural control of Zr materials during fabrications.

Therefore, in the present work, commercially pure Zr sheets were selected as the experimental materials, which were β air-cooled and then rolled to different reductions (10% and 50%) at room temperature. Their microstructures were well investigated by use of electron channeling contrast (ECC) imaging and electron backscatter diffraction (EBSD) techniques based on a field emission gun scanning electron microscope, with particular attentions paid to the misorientation characteristics associated with specific deformation modes. Analyses based on local misorientations were also performed so as deformation-induced residual strains in various specimens could be evaluated.

2 Experimental

The as-received materials were 2-mm-thick commercially pure Zr (cp-Zr) sheets with major impurities of (in wt.%) of 1.15 Hf, <0.08 Fe+Cr and 0.15 O. The starting microstructure of the as-received sheets was noted to be featured by well-equiaxed grains after sufficient recrystallization, which has already been documented in our recent work [31]. The β transus temperature of the cp-Zr was determined to be about 960°C. The as-received materials were heat-treated at 1000°C for 10 min under vacuum in a box furnace and then cooled in flowing air. After the β air cooling, two sheets were rolled at room temperature by 5% per pass to thickness reductions of 10% and 50%, respectively. Rectangular specimens with dimensions of 12 and 10 mm along rolling and transverse directions (RD and TD) were cut from both the β-air-cooled and the rolled sheets.

A Zeiss Sigma HD field emission gun scanning electron microscope (FEG-SEM) was employed to perform microstructural characterization for these specimens. ECC images based on back-scattered electrons were taken to reveal both composition- and orientation-related features [32–34]. An EBSD system attached to the FEG-SEM was used to further quantify crystallographic orientations of specific microstructures of the specimens. The EBSD system consisted of an Oxford Instruments NordlysMax2 detector with AZtec 2.4 and Channel 5 software packages for data acquisition and post processing, respectively. Prior to such microstructural characterization, RD-ND planes of the specimens were mechanically ground by SiC abrasive paper and then electropolished in a mixed solution of 10 mL perchloric acid, 20 mL butyl cellosolve and 70 mL methanol at 20 V and −30°C for 30–60 s.

3 Results and discussion

Figure 1 presents direct microstructural observations (ECC images) for the β-air-cooled and the rolled specimens. After the β→α air cooling treatment, grains are found to be mainly presented in lamellar shape (Figure 1(a)), different from the equiaxed grains in the as-received material [31]. The average width of the lamellar grains is measured to be ~8.5 μm. A magnified observation reveals that a number of second phase particles (SPPs) are distributed along boundaries of the lamellar grains, as arrowed in Figure 1(b). This suggests the occurrence of diffusion of impurity elements during the β air cooling and such microstructural features correspond to Widmanstätten structures. In fact, similar lamellar structures have been commonly seen in many β-treated Zr alloys and the SPPs at boundaries were determined to be Zr $(Fe, Cr)_2$ Laves phases [9,11]. Since the impurity content (especially Fe and Cr) in the cp-Zr is relatively limited, the volume fraction of the SPPs in the AC specimen is estimated to be very small (<0.5%).

After 10% rolling, most lamellar grains seem to be aligned and elongated slightly towards the RD, along with the presence of twin-like structures in some locations (Figure 1(c)). A closer observation in Figure 1(d) shows that the twin-like structures have distinct contrasts from the matrix with serrated boundaries between them. Sizes of the twin-like structures are found to vary a lot, ranging from several to near a hundred micrometers in length. For the 50%-rolled specimen, Figure 1(e) reveals that the prior Widmanstätten structures are heavily deformed and kinked, with the lamellar grains evidently elongated towards the RD. Grain refinement and subdivision could be noted after a magnified observation in Figure 1(f), as suggested by the greatly heterogeneous contrasts inside each lamellar grain.

EBSD band contrast (BC) and inverse pole figure (IPF)

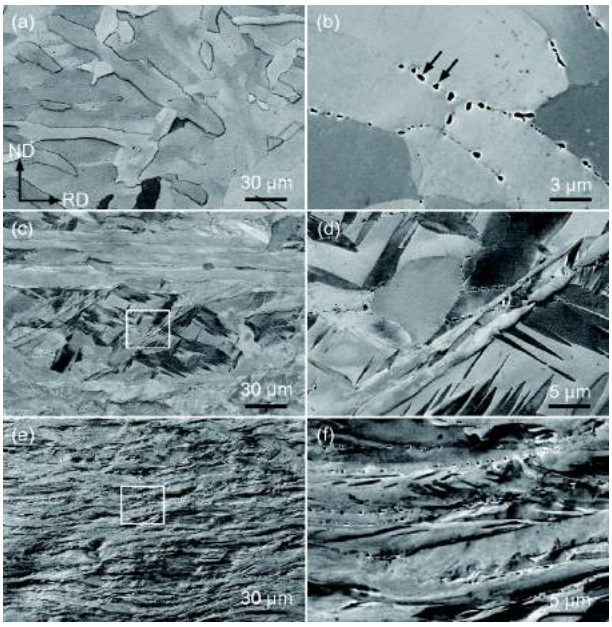

Figure 1 ECC images of the ((a), (b)) β-air-cooled, ((c), (d)) the 10%-rolled and ((e), (f)) the 50%-rolled specimens. Arrows in (b) indicate second phase particles; (d) and (f) correspond to boxed regions in (c) and (e), respectively.

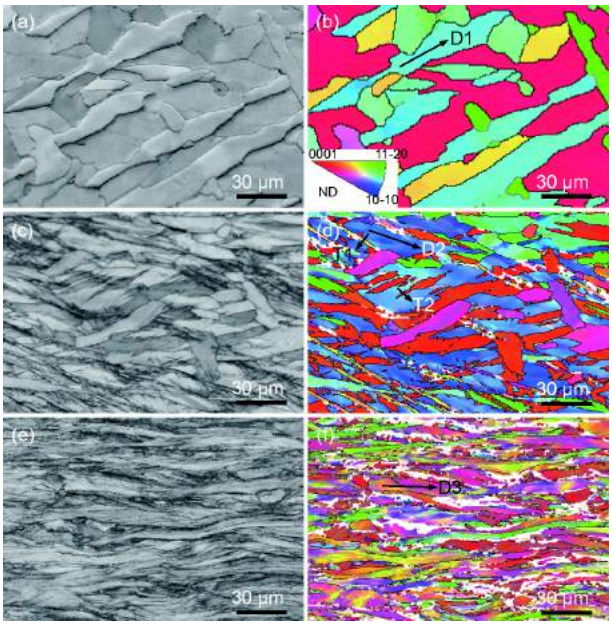

Figure 2 (Color online) EBSD BC maps of (a) the β-air-cooled, (c) the 10%-rolled and (e) the 50%-rolled specimens; (b), (d) and (f) IPF maps corresponding accordingly to (a), (c) and (e), with HABs and LABs indicated by black and gray lines, respectively.

maps of various specimens are displayed in Figure 2. Figure 2(a) reveals that high-quality Kikuchi patterns are obtained for the β-air-cooled specimen, suggesting hardly any residual stresses/strains. In Figure 2(b), a rather uniform orientation (color) is noted for each lamellar grain enclosed by high angle boundaries (HABs, θ>15°). Very few low angle boundaries (LABs, 2°<θ<15°) can be found in the grain interior, confirming the suppression of dislocation activities during the β→α air cooling. Indeed, the structural discrepancy of β and α phases might induce stresses during the allotropic phase transformation, leading to active slip and/or twinning like in the case of martensitic transformation [10,12]. In the present work, however, the relatively slow air cooling could allow such accumulated stresses to be sufficiently relaxed by creep processes at high temperature [35].

For the 10%-rolled specimen, varied image qualities in Figure 2(c) suggest the occurrence of heterogeneous plastic deformation. From Figure 2(d), the twin-like structures revealed in Figure 1(d) can also be seen, with their orientations confirmed to be largely different from the matrix. In addition, in contrast with the insignificance of LABs in the β-air-cooled specimen, a moderate number of LABs are found to be dispersed inside both the matrix (lamellar grains) and the twin-like structures. As a result, the orientation (color) of a specific grain is no longer uniform. After increasing the rolling reduction to 50%, the heavily deformed structures revealed in Figure 1(e) are again noted in Figure 2(e), from which the exclusive alignment towards the RD can be clearly seen for length directions of the lamellar grains. Moreover, Figure 2(f) reveals greatly denser LABs inside each grains and much severer grain subdivision than in the 10%-rolled case. Also note that twin-like structures observed in the 10%-rolled specimen (Figure 2(d)) are no longer evident due probably to their morphological destruction by extensive dislocation movements.

Misorientation variations associated with typical microstructural characteristics in various specimens are presented in Figure 3. Figure 3(a) shows cumulative misorientation angles (CMAs) inside specific lamellar grains in different specimens. For the β-air-cooled specimen, the CMA is generally found to be low (<2°), corresponding to a minimal orientation gradient (<0.1° μm^{-1}). After a slight rolling (10% rolling), about 9° can be accumulated along a 30 μm distance inside a lamellar grain, giving a moderate orientation gradient (~0.3° μm^{-1}). Inside the lamellar grains of the 50%-rolled specimen, Figure 3(a) reveals that the CMA can be rapidly increased to near 30° for the same distance, indicating a large orientation gradient of ~1.0° μm^{-1}. Note that developments of the orientation gradient during rolling are found to be consistent with increased densities of LABs (Figure 2). Also, the CMAs inside lamellar grains in both the rolled specimens are found to be gradually increased. One can thus deduce that the gradual lattice rotations during rolling should be induced by continuous dislocation slip rather than twinning [22,24].

With respect to twin-like structures appeared in the 10%-rolled specimen (Figure 2(d)), typical misorientation variations across their boundaries are also measured. As displayed in Figure 3(b) and (c), two types of misorientations (angle/axis pairs), i.e., ~35°/<10-10>and ~85°/<11-20>, are gen-

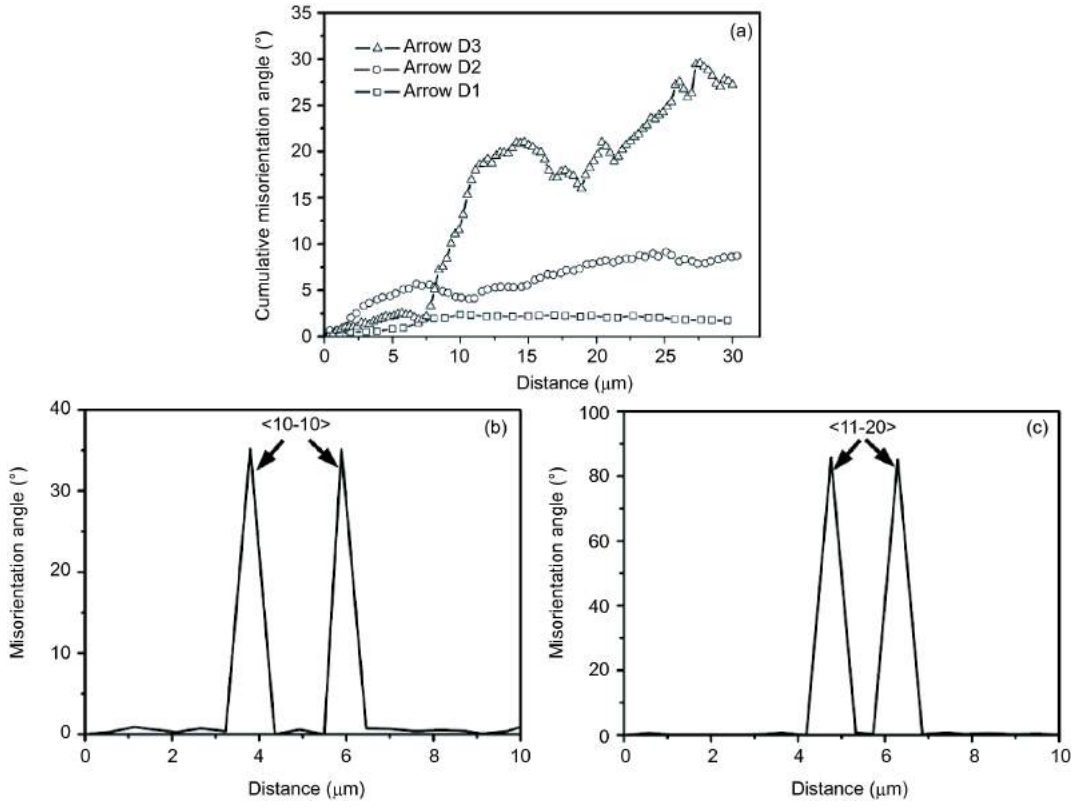

Figure 3 Cumulative misorientation angles along various measuring paths as arrowed in Figure 2. (a) D1-D3; (b) T1; (c) T2.

erally detected. They are found to be well coincident with crystallographic characteristics of {11-21}<11-2-6>and {10-12}<10-11> tensile twins (Table 1). It is thus known that such twin-like structures correspond to the two types of tensile twins in α-Zr. In an earlier work, Crépin et al. [36] also detected the two types of tensile twins in a β-treated Zr702 subjected to uniaxial tension. They reported that the measured critical resolved shear stress (CRSS) of the {10-12}<10-11> twins is much lower than that of the {11-21}<11-2-6> twins and thus allowed them to be more easily initiated.

In addition to the local misorientation characteristics revealed in Figure 3, Figure 4 presents global misorientation angle and rotation axis distributions of all the three specimens. For the β-air-cooled specimen, three peaks around 10°, 60° and 90° can be exclusively seen from Figure 4(a). Such a misorientation angle distribution has been commonly observed for Zr alloys after β-cooling [10,30,37]. In fact, the classical Burgers orientation relationship (OR) ($\{110\}_\beta$// $\{0001\}_\alpha$ and $<111>_\beta$//$<11\text{-}20>_\alpha$) predicts five specific misorientations between α variants generated by the same β orientation, i.e., 10.5°/<0001>, 60°/<11-20>, 60.8°/~<12-31>, 63.3°/~<44-83>and 90°/~<12-30>[30]. Examinations on rotation axes corresponding to the three peaks suggest that they are in good agreement with the five misorientations predicted by the Burgers OR. The peak around 60° can be

Table 1 Deformation modes operable in α-Zr and their basic parameters.

Deformation mode			Taylor rotation axis	Lattice rotation	Twinning shear
Twinning	Tensile	{10-12}<10-11>	<11-20>	85.22°	0.167
		{11-21}<11-2-6>	<10-10>	34.84°	0.627
	Compressive	{11-22}<11-2-3>	<10-10>	64.22°	0.225
		{10-11}<10-12>	<11-20>	57.05°	0.104
Slip	<a> type	{10-10}<11-20>	<0001>	Continuous	Not applicable
		{0002}<11-20>	<10-10>		
		{10-11}<11-20>	<10-12>		
	<c+a> type	{10-11}<11-23>	<13-8-53>		
		{11-21}<11-23>	<6-1-53>		

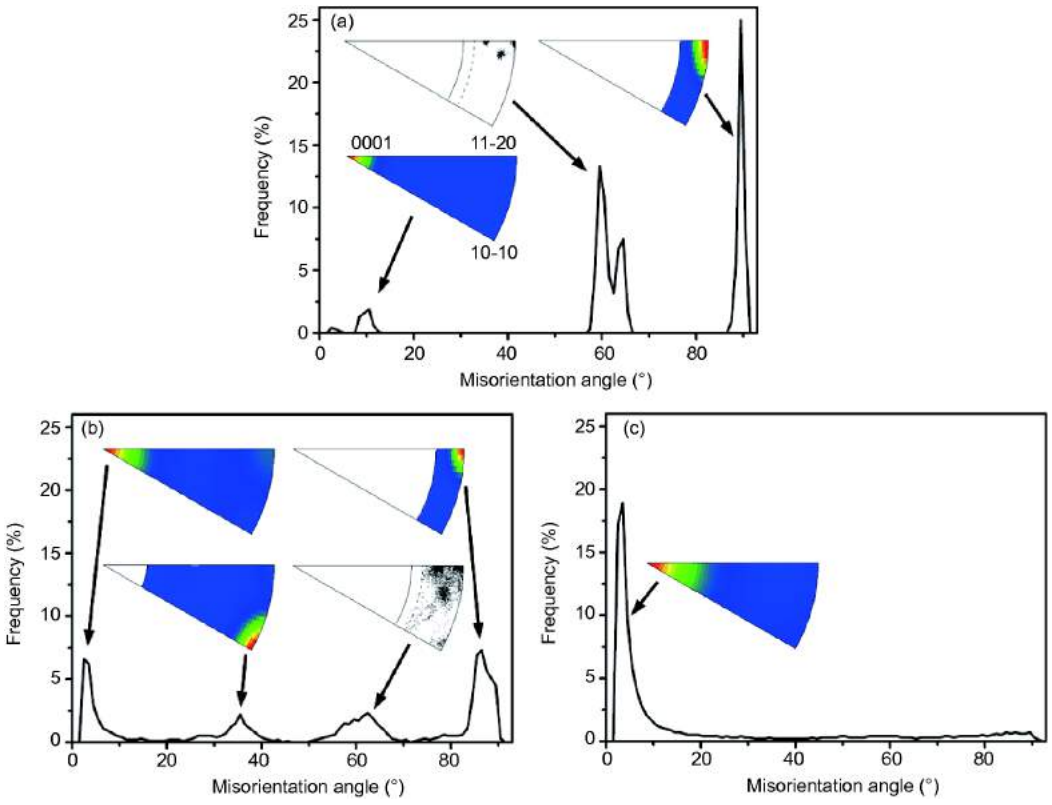

Figure 4 (Color online) Misorientation angle and rotation axis distributions of (a) the β-air-cooled, (b) the 10%-rolled and (c) the 50%-rolled specimens.

ascribed to an overlap of measured angles corresponding to the second, third and fourth Burgers misorientations (see ref. [30] for detailed illustration). One can know that the misorientation characteristic of the β-air-cooled specimen is completely resulted from the β→α phase transformation according to the Burgers OR.

For the 10%-rolled specimen, remarkable changes can be noted for its misorientation angle distribution (Figure 4(b)). The highest peak near 90° in the β-air-cooled specimen is largely reduced in intensity and slightly shifted towards lower angles. In fact, its new peak center is adjusted close to 85° with the rotation axis well concentrated on <11-20>. This suggests that the prior 90°/~<12-30> misorientation should have been largely destructed and overlapped with the ~85°/<11-20> misorientation due to the appearance of dense {10-12}<10-11> twins (Figure 2(d)). The prior peak around 60° is also heavily decayed, with evidently spread angles and rotation axes. A new peak around 35° appears with rotation axes focused on <10-10>, corresponding to that of {11-21}<11-2-6> twins. The presence of this peak also suggests the abundance of the {11-21}<11-2-6>twins in the 10%-rolled specimen. This is in contrast with the case that no twins were found in a typically textured pure Zr sheet subjected to the same rolling [22], in spite of its larger grain sizes (~9.6 μm on average). This may be mainly attributed to a textural difference between them. Indeed, the β-air-cooled specimen in this work was found to possess a relatively random texture (documented in ref. [7]), which would contain more favorable orientations for twinning. With respect to low misorientation angles, the prior peak near ~10° seems to be completely suppressed and replaced by a new one focused on lower angles (3°–5°). The new low-angle peak should mainly correspond to those LABs produced by dislocation movements, as shown in Figure 2(d). According to Table 1, activated slip modes leading to these low angles can be probed by considering their corresponding rotation axes (more detailed illustration can be seen in ref. [38]). As revealed in Figure 4(b), a highly concentrated rotation axis of <0001> is found for these low angles, suggesting prismatic slip ({10-10}<11-20>) of <a> dislocation as the main slip mode. In fact, compared with other operable slip systems, prismatic slip is usually the easiest to be initiated during deformation due to its much lower CRSS [39].

With increasing rolling reduction to 50%, all the prior high-angle peaks appear to be completely suppressed, with only one low-angle peak highly intensified (Figure 4(c)). Clearly, twinning should no longer play a key role in the deformation process, which could reply more on slip instead. A similar phenomenon was earlier reported for a Zircaloy-2 subjected to different degrees of uniaxial compression [40]. The insignificance of twinning at later stages of deformation can be ascribed to both changed crystallographic texture and

refined grains by earlier twins. Figure 4(c) also reveals that the rotation axes corresponding to the left low-angle peak remain concentrated on the <0001>, indicating the same predominant deformation mode (prismatic slip) as that in 10%-rolled specimen. Nevertheless, since the prismatic slip could only accommodate stains along a-axes of hcp structures, other deformation modes with the ability of accommodating strains along grain c-axes should be needed. Such a role could be played by twinning at the early state of rolling (Figures 2(d) and 4(b)). However, the absence of twins in the 50%-rolled specimen suggests that pyramidal slip of <c+a> dislocations should have been activated to some extent, in spite of their higher CRSSs [39]. This is also supported by the earlier work [41] that presented experimental evidences of activation of {10-11}<11-23> slip in a pure Zr deformed at room temperature.

Figure 5 presents EBSD kernel average misorientation (KAM) maps, which are reconstructed in terms of local misorientation characteristics and known to be capable of directly reflect distributions of residual strains in the specimen interiors [42]. For each KAM map, the maximum misorientation is selected to be 5° with only the three nearest neighbors considered. Figure 5(a) reveals a relatively low and uniform KAM distribution throughout the microstructure of the β-air-cooled specimen, with an average KAM calculated to be 0.24° (Figure 5(b)). The value is comparable to that of fully recrystallized grains [43], suggesting few residual strains after the slow β→α cooling, consistent with the above analysis based on Kikuchi patterns (Figure 2(a)). As above mentioned, this could be ascribed to sufficient relaxation of stresses/strains by creep at high temperature [35]. For the 10%-rolled specimen, the KAM distribution is found to become highly heterogeneous in Figure 5(c). A comparison between Figures 2(d) and 5(c) suggests that the KAM is generally larger near grain/twin boundaries than inside them. This can be understood that dislocations are easily to be piled up in front of the grain or twin boundaries (both of them belong to HABs) during the rolling. The increased average KAM (0.72°) and the more spread distribution shown in Figure 5(d) clearly manifest the presence of residual strains. After the heavier deformation (50% rolling), larger KAM can be noticed throughout the specimen microstructure, as shown in Figure 5(e). The average KAM of the 50%-rolled specimen is calculated to be 1.52° (more than double that of the 10%-rolled specimen) with its distribution histogram spreading more towards higher angles (Figure 5(f)). According to the KAM results, much larger residual strains can be expected for the 50%-rolled specimen. As twinning is well suppressed, the residual strains should be essentially attributed to extensive dislocation slip (both prismatic and pyramidal systems). Also, different from the preferred activities of dislocations near HABs during the 10% rolling (Figure 5(c)), the pervasive

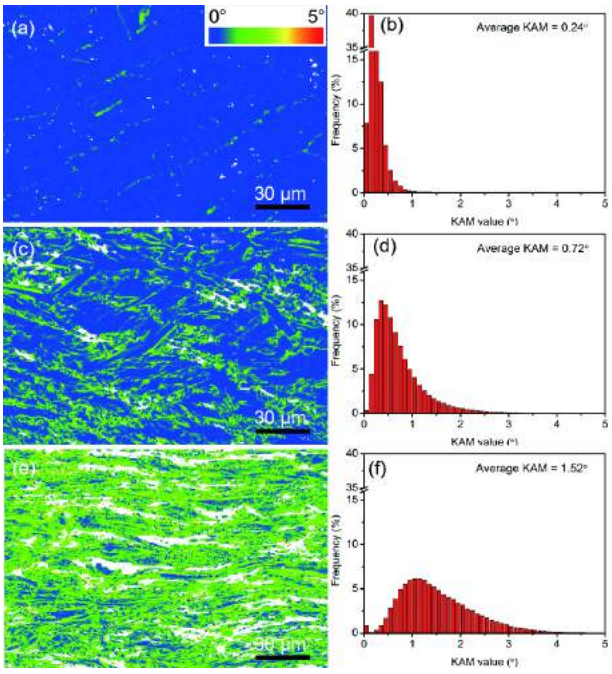

Figure 5 (Color online) KAM maps of (a) the β-air-cooled, (c) the 10%-rolled and (e) the 50%-rolled specimens; (b), (d) and (f) KAM distribution histograms corresponding accordingly to (a), (c) and (e).

existence of residual strains (Figure 5(e)) indicates active dislocation slip both inside grains and near their boundaries. This can also be evidenced by the large orientation gradient in lamellar grain interiors, as revealed in Figure 3(a).

4 Conclusions

(1) The β-air-cooled specimen possesses a Widmanstätten structure featured by lamellar grains with scattered orientations. During the 10% rolling, both active twinning and slip occur; however, only dislocation slip is the dominant deformation mode after increasing the rolling reduction to 50%, with the lamellar grains highly elongated and aligned towards the RD.

(2) Three typical misorientation angle peaks corresponding to the Burgers misorientations are noted for the β-air-cooled specimen. After the 10% rolling, all the three peaks are largely decayed with the appearance of new low-angle (~3°–5°) and high-angle (~35° and ~85°) peaks, resulting from prismatic slip and tensile twinning ({11-21}<11-2-6> and {10-12}<10-11>), respectively. Only one strong low-angle peak related to prismatic slip is presented after increasing the rolling reduction to 50%, with all other peaks disappeared.

(3) Hardly any residual strains are found in the β-air-cooled specimen, which should be related to sufficient relaxation during slow cooling. Residual strains introduced by 10% rolling are heterogeneously distributed near grain/twin

boundaries due to preferred dislocation pile ups. After heavier deformation (50% rolling), much larger residual strains are noted with the pervasive existence throughout the specimen microstructure.

This work was supported by the Fundamental and Cutting-Edge Research Plan of Chongqing (Grant Nos. cstc2017jcyjAX0114 & cstc2016jcyjA0434) and the National Natural Science Foundation of China (Grant Nos. 51401040, 51601075 & 51601165).

1 Duan Z G, Yang H L, Satoh Y, et al. Current status of materials development of nuclear fuel cladding tubes for light water reactors. Nucl Eng Des, 2017, 316: 131–150
2 Zinkle S J, Was G S. Materials challenges in nuclear energy. Acta Mater, 2013, 61: 735–758
3 Zhou F Y, Qiu K J, Li H F, et al. Screening on binary Zr–1X (X=Ti, Nb, Mo, Cu, Au, Pd, Ag, Ru, Hf and Bi) alloys with good *in vitro* cytocompatibility and magnetic resonance imaging compatibility. Acta Biomater, 2013, 9: 9578–9587
4 Daymond M R, Holt R A, Cai S, et al. Texture inheritance and variant selection through an hcp-bcc-hcp phase transformation. Acta Mater, 2010, 58: 4053–4066
5 Hiwarkar V D, Sahoo S K, Samajdar I, et al. Defining recrystallization in pilgered Zircaloy-4: From preferred nucleation to growth inhibition. J Nucl Mater, 2011, 412: 287–293
6 Murty K L, Charit I. Texture development and anisotropic deformation of zircaloys. Prog Nucl Energy, 2006, 48: 325–359
7 Chai L J, Luan B F, Chen B F, et al. Concurrent inheritance of microstructure and texture after slow β→α cooling of commercially pure Zr. Sci China Tech Sci, 2016, 59: 1771–1776
8 Kim H G, Baek J H, Kim S D, et al. Microstructure and corrosion characteristics of Zr-1.5Nb-0.4Sn-0.2Fe-0.1Cr alloy with a β-annealing. J Nucl Mater, 2008, 372: 304–311
9 Massih A R, Andersson T, Witt P, et al. Effect of quenching rate on the β-to-α phase transformation structure in zirconium alloy. J Nucl Mater, 2003, 322: 138–151
10 Yang H L, Kano S, Matsukawa Y, et al. Effect of molybdenum on microstructures in Zr-1.2Nb alloys after β-quenching and subsequently 873 K annealing. Mater Des, 2016, 104: 355–364
11 Ammar Y B, Aoufi A, Darrieulat M. Influence of the cooling rate on the texture and the microstructure of Zircaloy-4 studied by means of a Jominy end-quench test. Mater Sci Eng-A, 2012, 556: 184–193
12 Ahmmed K F, Daymond M R, Gharghouri M A. Microstructural evaluation and crystallographic texture modification of heat-treated zirconium Excel pressure tube material. J Alloys Compd, 2016, 687: 1021–1033
13 Yang H L, Matsukawa Y, Kano S, et al. Investigation on microstructural evolution and hardening mechanism in dilute Zr-Nb binary alloys. J Nucl Mater, 2016, 481: 117–124
14 Yuan G H, Cao G Q, Yue Q, et al. Formation and fine-structures of nano-precipitates in ZIRLO. J Alloys Compd, 2016, 687: 451–457
15 Yang H L, Shen J J, Kano S, et al. Effects of Mo addition on precipitation in Zr-1.2Nb alloys. Mater Lett, 2015, 158: 88–91
16 Liang J L, Zhang M, Ouyang Y F, et al. Contribution on the phase equilibria in Zr-Nb-Fe system. J Nucl Mater, 2015, 466: 627–633
17 Yao M Y, Shen Y F, Li Q, et al. The effect of final annealing after β-quenching on the corrosion resistance of Zircaloy-4 in lithiated water with 0.04 M LiOH. J Nucl Mater, 2013, 435: 63–70
18 Liu C, Li G, Yuan F, et al. Stacking faults in Zr(Fe, Cr)$_2$ Laves structured secondary phase particle in Zircaloy-4 alloy. Nanoscale, 2018, 10: 2249–2254
19 Hu X Y, Zhao H L, Ni S, et al. Grain refinement and phase transition of commercial pure zirconium processed by cold rolling. Mater Charact, 2017, 129: 149–155
20 Fuloria D, Kumar N, Jayaganthan R, et al. An investigation of effect of annealing at different temperatures on microstructures and bulk textures development in deformed Zircaloy-4. Mater Charact, 2017, 129: 217–233
21 Yang H L, Kano S, Matsukawa Y, et al. Study on recrystallization and correlated mechanical properties in Mo-modified Zr-Nb alloys. Mater Sci Eng-A, 2016, 661: 9–18
22 Chai L J, Luan B F, Xiao D P, et al. Microstructural and textural evolution of commercially pure Zr sheet rolled at room and liquid nitrogen temperatures. Mater Des, 2015, 85: 296–308
23 Li M H, Ma M, Liu W C, et al. Recrystallization behavior of cold-rolled Zr 702. J Nucl Mater, 2013, 433: 6–9
24 Kumar M K, Vanitha C, Samajdar I, et al. Deformation texture and microtexture developments in a cold rolled single phase hexagonal Zircaloy 2. Mater Sci Tech, 2006, 22: 331–342
25 Randle V. Grain boundary engineering: An overview after 25 years. Mater Sci Tech, 2010, 26: 253–261
26 Watanabe T. Grain boundary engineering: Historical perspective and future prospects. J Mater Sci, 2011, 46: 4095–4115
27 Bozzolo N, Chan L, Rollett A D. Misorientations induced by deformation twinning in titanium. J Appl Crystlogr, 2010, 43: 596–602
28 Hu Y, Randle V. An electron backscatter diffraction analysis of misorientation distributions in titanium alloys. Scripta Mater, 2007, 56: 1051–1054
29 Chai L J, Chen B F, Zhou Z M, et al. A special twin relationship or a common Burgers misorientation between α plates after β quenching in Zr alloy? Mater Charact, 2015, 104: 61–65
30 Chai L J, Luan B F, Zhang M, et al. Experimental observation of 12 α variants inherited from one β grain in a Zr alloy. J Nucl Mater, 2013, 440: 377–381
31 Chai L J, Chen B F, Wang S Y, et al. Microstructural changes of Zr702 induced by pulsed laser surface treatment. Appl Surf Sci, 2016, 364: 61–68
32 Zaefferer S, Elhami N N. Theory and application of electron channelling contrast imaging under controlled diffraction conditions. Acta Mater, 2014, 75: 20–50
33 Chai L J, Wu H, Wang S Y, et al. Characterization of microstructure and hardness of a Zr-2.5Nb alloy surface-treated by pulsed laser. Mater Chem Phys, 2017, 198: 303–309
34 Chai L J, Wang S Y, Wu H, et al. α→β Transformation characteristics revealed by pulsed laser-induced non-equilibrium microstructures in duplex-phase Zr alloy. Sci China Tech Sci, 2017, 60: 1255–1262
35 Tomé C N, Christodoulou N, Turner P A, et al. Role of internal stresses in the transient of irradiation growth of Zircaloy-2. J Nucl Mater, 1996, 227: 237–250
36 Crépin J, Bretheau T, Caldemaison D. Plastic deformation mechanisms of β treated zirconium. Acta Metall Mater, 1995, 43: 3709–3719
37 Chai L J, Wang S Y, Wu H, et al. Bimodal plate structures induced by pulsed laser in duplex-phase Zr alloy. Sci China Tech Sci, 2017, 60: 587–592
38 Chun Y B, Battaini M, Davies C H J, et al. Distribution characteristics of in-grain misorientation axes in cold-rolled commercially pure titanium and their correlation with active slip modes. Metall Mat Trans A, 2010, 41: 3473–3487
39 Xu F, Holt R A, Daymond M R. Modeling texture evolution during uni-axial deformation of Zircaloy-2. J Nucl Mater, 2009, 394: 9–19
40 Sahoo S K, Hiwarkar V D, Samajdar I, et al. Deformation twinning in zircaloy 2. Mater Sci Tech, 2010, 26: 104–114
41 Numakura H, Minonishi Y, Koiwa M. <-1-123>{10-11}} slip in zirconium. Philos Mag A, 1991, 63: 1077–1084
42 Wright S I, Nowell M M, Field D P. A review of strain analysis using electron backscatter diffraction. Microsc Microanal, 2011, 17: 316–329
43 Guo N, Li D R, Yu H B, et al. Annealing behavior of gradient structured copper and its effect on mechanical properties. Mater Sci Eng-A, 2017, 702: 331–342